Monitoring calcium in turtle hair cells with a calcium-activated potassium channel

Thomas R. Tucker and Robert Fettiplace*

Department of Neurophysiology and Neuroscience Training Program, University of Wisconsin Medical School, Madison, WI 53706, USA

1. An apamin-sensitive Ca^{2+}-activated K^+ channel was characterized in turtle hair cells and utilized to monitor submembranous intracellular Ca^{2+} and to evaluate the concentration of the mobile endogenous calcium buffer.

2. Isolated hair cells were voltage clamped with whole-cell patch electrodes filled with a Cs^+-based intracellular solution to block the large-conductance Ca^{2+}-activated K^+ (BK) channel. Ca^{2+} currents evoked by depolarization were followed by inward tail currents lasting several hundred milliseconds. Both the Ca^{2+} current and slow tail current were abolished by nifedipine.

3. The tail current was carried by K^+ and Cs^+ (relative permeabilities $P_{Cs}/P_K = 0{\cdot}22$), and was fully blocked by 0·1 μM apamin and half blocked by 5 mM external TEA. These properties suggest the tail current flows through a Ca^{2+}-activated K^+ channel distinct from the BK channels.

4. Intracellular Ca^{2+} was imaged with a confocal microscope in hair cells filled with the indicator Calcium Green-5N introduced via the patch pipette. Increases in Ca^{2+} evoked by depolarization were localized to hotspots on the basolateral surface of the cell. The time course of the tail current closely matched the fast component of the fluorescence monitored at a hotspot.

5. Ca^{2+}-ATPase pump inhibitors thapsigargin, 2,4-di-(t-butyl)hydroquinone (BHQ) and vanadate, which are known to influence calcium regulation in turtle hair cells, prolonged the time course of the tail current, supporting the idea that the channel monitors cytoplasmic Ca^{2+}.

6. The mobile endogenous buffer was estimated by combining perforated-patch and whole-cell recordings on a single cell. After recording tail currents with an amphotericin-perforated patch, the patch was ruptured to obtain the whole-cell mode, thus allowing washout of soluble cytoplasmic proteins and exchange with pipette buffers. By varying the concentration of Ca^{2+} buffer in the pipette, the mobile endogenous buffer was found to be equivalent to about 1 mM BAPTA.

A number of intracellular actions of ionized calcium (Ca^{2+}), including the triggering of neurotransmitter release in neurons or gating of Ca^{2+}-activated ion channels, occur near the plasma membrane. During the release of transmitter, it has been postulated that peak [Ca^{2+}] at presynaptic active zones may rapidly exceed 100 μM and elicit fusion of synaptic vesicles within a few hundred microseconds after excitation (Smith & Augustine, 1988). While imaging experiments verify large and rapid Ca^{2+} changes at the membrane (Llinás, Sugimori & Silver, 1992; Tucker & Fettiplace, 1995), quantifying the exact spatial and temporal bounds has been difficult due to the restrictions imposed by light microscopy and the properties of the calcium indicators (Neher & Augustine, 1992; Pawley, 1995). An electrophysiological method for monitoring Ca^{2+} at the membrane, which can be used to supplement imaging data, takes advantage of Ca^{2+}-activated ion channels (Barish & Thompson, 1983). This technique has been applied in frog saccular hair cells to show that the maximum current through large-conductance Ca^{2+}-activated K^+ (BK) channels depended on a mobile endogenous buffer (Roberts, 1993). The experiment relied on comparing currents obtained using perforated-patch recordings with currents recorded in the whole-cell mode, but had the limitation that the two types of measurement were derived from different cells. Here, we characterize a Ca^{2+}-activated K^+ current that may

* To whom correspondence should be addressed.

be carried through the small-conductance Ca^{2+}-activated K^+ (SK) channels previously observed in detached patches (Art, Wu & Fettiplace, 1995). The K^+ current's gating has a time course similar to that of Ca^{2+} signals imaged with a confocal microscope (Tucker & Fettiplace, 1995), suggesting that it reports the local Ca^{2+} concentration. We have used this K^+ current to obtain evidence about the mechanism of Ca^{2+} extrusion in turtle hair cells and also to measure the properties of the cells' mobile endogenous Ca^{2+} buffer.

METHODS

Electrophysiology

Experiments were performed on hair cells isolated from the basilar papilla of the turtle *Trachemys scripta elegans* (Art & Fettiplace, 1987). The turtle was decapitated and the basilar papilla dissected out and enzymatically dissociated in a saline containing 0·1 mM $CaCl_2$ to which had been added (mg ml^{-1}): 0·5 papain (Calbiochem), 0·1 bovine serum albumin and 0·5 L-cysteine. Isolated cells were plated in an extracellular solution containing (mM): 125 NaCl, 4 KCl, 5 $CaCl_2$, 10 glucose, 10 NaHepes, pH 7·6, onto a clean coverslip mounted on the stage of a Zeiss Axiovert 10 microscope. Borosilicate whole-cell patch electrodes were usually filled with an intracellular solution containing (mM): 125 CsCl, 3 $MgCl_2$, 2·5 Na_2ATP, 1 EGTA, 5 Hepes, neutralized to pH 7·2 with CsOH. In later experiments to study the endogenous buffer, EGTA was replaced by various concentrations of BAPTA (0·1–5 mM) as the Ca^{2+} buffer. Cells were voltage clamped at a holding potential of −80 mV and step depolarizations were elicited for durations of between 0·1 and 1·5 s at a repetition rate of 1/90 s. External perfusion of a cell was accomplished with an assembly of pan pipes connected to a perfusion pump, and individual channels were remotely selected with a miniature solenoid valve. Membrane currents were stored on a Sony PC-108M DAT recorder at a band width of 20 kHz. Experiments were performed at a temperature of about 23 °C. Unless otherwise stated, results are expressed as means ± 1 standard deviation.

The resonant frequencies of the hair cells used, assessed both from the height of the hair bundle and the Ca^{2+} current's amplitude (Art & Fettiplace, 1987), were between about 150 and 300 Hz. The peak Ca^{2+} current ranged from 400 to 1200 pA in 5 mM external Ca^{2+} saline. There were often changes in the amplitude of the Ca^{2+} current and tail current during the first few minutes of recording after rupturing the patch to obtain the whole-cell configuration. Reasons for the drift may include the washout of endogenous mobile buffers and other cell constituents. To control for this effect, between 5 and 10 min was allowed after breakthrough for the currents to stabilize before any experimental manipulations were begun. Sodium vanadate (Aldrich) and thapsigargin (Calbiochem) were applied intracellularly through the recording pipette, but in order to obtain both control and test recordings, the electrode was tip-filled with normal intracellular solution and back-filled with intracellular solution containing the drug. An amount of normal intracellular solution was drawn into the tip by suction to allow roughly 15 min of recording before arrival by diffusion of the test solution. A typical recording time in these experiments was 45 min (range, 35–60 min). Extracellular application of thapsigargin produced identical results to intracellular application, but the method was discontinued since the cells sometimes appeared to be contaminated by trace amounts leaking from the perfusion pipe prior to application. Tetraethylammonium (TEA) chloride, obtained from Aldrich, and 2,4-di-(t-butyl)hydroquinone (BHQ), apamin and nifedipine, all supplied by Calbiochem, were applied extracellularly. Since the tail current's shape was complex and not easily fitted by a sum of exponentials, two methods were employed for analysing its time course. Its duration was quantified by measuring the time required for the tail to decay to 1/e from the peak amplitude at the end of the pulse. Alternatively, the tail current was integrated by calculating the area enclosed to the zero-current level for up to 5 s from the end of the pulse.

Perforated-patch recordings were performed using a previously published method (Rae, Cooper, Gates & Watsky, 1991). The intracellular solution contained (mM): 15 CsCl, 110 caesium aspartate, 3 $MgCl_2$, 2·5 Na_2ATP, 0·1–5 Cs_4-BAPTA, 5 NaHepes, neutralized to pH 7·2 with CsOH. The caesium aspartate was reduced to 105 mM in the solution containing 5 mM BAPTA. This stock solution was mixed with 240 $\mu g\ ml^{-1}$ amphotericin B (Calbiochem) and 0·1% dimethylsulphoxide made fresh for each experiment. The patch pipette was tip-filled with the stock solution, and back-filled with the amphotericin to prevent leakage into the bath. Access resistances were typically 15–20 MΩ in perforated-patch mode, but were smaller after the breakthrough into whole-cell mode detected by a sudden increase in the current transient monitored with 20 mV pulses from −80 mV. Membrane potentials were corrected for the junction potential between the caesium aspartate solution and the external saline, the true potentials being about 10 mV more hyperpolarized than those measured with CsCl intracellular solutions. The time constant, τ, of exchange between the pipette and intracellular environment was calculated from an empirical formula, $\tau = 0{\cdot}6R_aM^{1/3}$, where τ is in seconds, R_a, the pipette access resistance, is in megaohms and M, the molecular mass of the diffusing species, is in daltons. The formula was determined (Pusch & Neher, 1988) on chromaffin cells that have a similar volume and geometry to hair cells. With a 10 MΩ access resistance, the time constant of diffusional exchange would be about 45 s for BAPTA with $M = 500$ Da, and 3 min for a protein like calbindin with $M = 28$ kDa. After rupturing a perforated patch, all recordings illustrated were continued for 20 min to ensure exchange of the cell constituents with the pipette solution.

Imaging of intracellular calcium

Intracellular Ca^{2+} was monitored with Calcium Green-5N (Molecular Probes), a low-affinity fluorescent indicator with a binding constant, K_D, of 25 μM, using techniques previously described (Tucker & Fettiplace, 1995). Hair cells were loaded with 0·1 mM hexapotassium salt of the indicator by adding it to the pipette solution. Cells were illuminated with the 488 nm line of a 300 mW argon ion laser and the fluorescence images were collected via a 515 nm long-pass filter by means of an Odyssey video-rate laser scanning confocal microscope (Noran Instruments, Middleton, WI, USA) connected via the bottom TV (Keller) port of the Zeiss optical microscope. Cells were viewed with a 40 × 0·75 NA plan neofluar objective, and further magnified with either a ×2·5 optivar or the Odyssey's computer-controlled zoom. The thickness of the confocal section was determined by the detection slit width, which was set to either 15 or 50 μm, the narrower slit corresponding to an axial resolution of about 3·5 μm. In order to ensure a stable baseline the laser intensity was minimized. The Odyssey generated an RS-170 video-rate signal at 30 frames s^{-1} and the vertical synchronization pulse of the video signal was employed to trigger the voltage-clamp pulses in order to synchronize their timing with the start of an image. The images were recorded on videocassette using a Sony S-VHS recorder (SVO-9500MD). Subsequent analysis was performed with the MetaMorph software package (Universal Imaging, West Chester, PA, USA) following capture of sequential images into memory of a

pentium PC equipped with a Matrox LC image board. To follow the time course of a fluorescence change, the brightness-over-time function in MetaMorph was applied to small regions of the cell, normally of diameter 20 pixels, equivalent to about 2 μm.

RESULTS

Ionic selectivity and pharmacology of a slow tail current

Current through the large-conductance Ca^{2+}-activated K^+ (BK) channel was blocked with a Cs^+-based intracellular solution in order to isolate the voltage-dependent Ca^{2+} current. The turtle hair cell's Ca^{2+} current is carried by L-type Ca^{2+} channels that activate in less than 1 ms, do not inactivate and have tails with time constants of well under 0·5 ms on repolarization to −80 mV (Art & Fettiplace, 1987). Figure 1*A* shows responses to voltage steps from −80 to −20 mV for durations of 300–900 ms. With such extended depolarizations, the current declined during the step, and there was a prolonged inward tail current lasting several hundred milliseconds on repolarization. We shall demonstrate that both the sag during the step and the slow tail current reflect the recruitment of a Ca^{2+}-activated K^+ conductance that can be blocked by the bee toxin apamin (Fig. 3). The slow tail current was present in the majority of recordings from mid-frequency hair cells and its amplitude and duration increased with pulse length. However, there was some variability in its size between cells which, under comparable conditions, ranged from about 0·1 to 0·8 nA.

When *N*-methylglucamine (NMG) was used as the major intracellular cation, the sag in the current was absent but the tails were largely unaffected (Fig. 1*B*). This result argues that the sag was not due to inactivation of the calcium current, but rather the activation of an outward current. It will be shown that this outward current flows through a Ca^{2+}-activated K^+ channel permeable to both Cs^+ and K^+ but not NMG. A plausible scheme is that when the cell is depolarized, Ca^{2+} accumulates at the membrane and activates the channels causing outward flow of current carried predominantly by Cs^+; when the cell is repolarized, K^+-dominated inward current flows as the channels deactivate during Ca^{2+} removal. Both the sag during the pulse and the slow tail current are caused by the same channel, the ionic selectivity of which was determined by substituting for each of the ions in the extracellular solution. The tail current was abolished when external K^+ was removed (Fig. 2*D*), but not when Na^+ was replaced with Li^+, or when Cl^- was replaced with methylsulphate (data not shown). The results of substitution of Li^+ for Na^+ indicate that the tail current is not a Na^+–Ca^{2+} exchange current as has been identified in photoreceptors (Yau & Nakatani, 1984; Hodgkin, McNaughton & Nunn, 1987). The absence of a Na^+–Ca^{2+} exchange current is consistent with other evidence that calcium removal from turtle hair cells occurs largely via a Ca^{2+}-ATPase pump (Tucker & Fettiplace, 1995; see also Fig. 8). The only effect of replacing Na^+ with Li^+ (or in some experiments with NMG) was a small reduction of the peak inward current (21 ± 10%, $n = 14$).

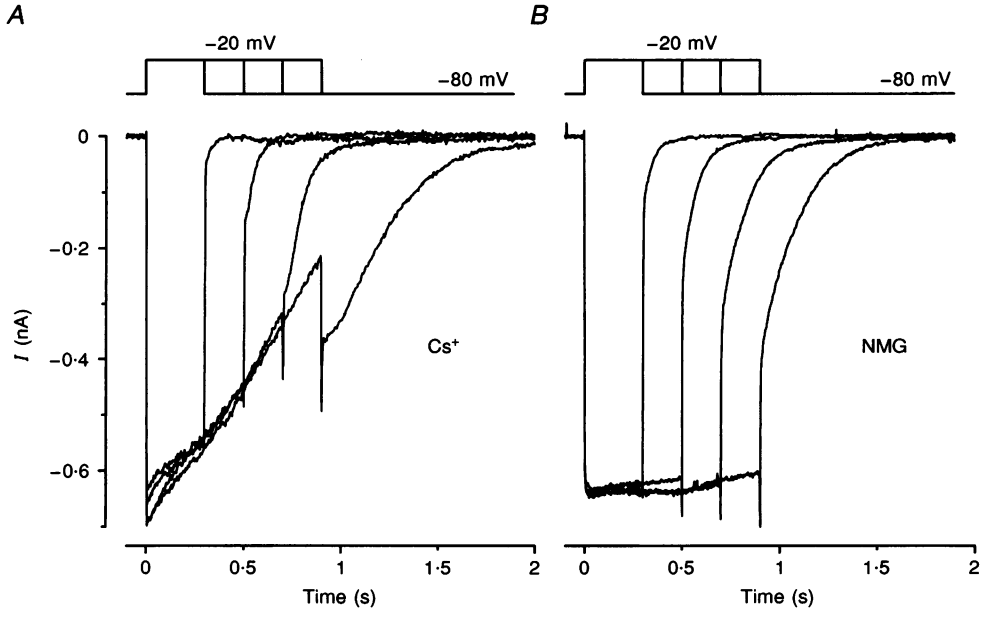

Figure 1. Membrane currents in isolated turtle hair cells recorded with intracellular solutions based on Cs^+ or *N*-methylglucamine (NMG)

A, currents recorded with Cs^+-based intracellular solution in response to depolarizing voltage steps from −80 to −20 mV, pulse durations ranging from 300 to 900 ms. The inward current decays throughout the depolarization, and is followed by a prolonged inward tail current that grows with pulse duration. *B*, superimposed currents from a different cell obtained using NMG-based intracellular solution with the same voltage protocol as in *A*. Note that the inward current does not decay during the pulse but the tail currents are of similar amplitude to those in *A*.

This reduction was evident at all potentials and did not entail a voltage shift in the Ca^{2+} current–voltage relationship. It seems likely that Li^+ substitution leads to block of the Ca^{2+} channels but the mechanism is presently unknown.

The reversal potential of the tail current was determined with a two-pulse protocol shown in Fig. 2. An initial pulse to −20 mV was issued to evoke a near-maximal Ca^{2+} current and to activate the slow tail current. A second pulse was delivered to potentials between −80 and +20 mV to change the driving force on the tail current, but which also changed the calcium current. Thus the current during the second pulse is the combination of a Ca^{2+} current and a tail current. The amplitude of the Ca^{2+} current at each potential was determined by constructing a Ca^{2+} current–voltage relationship with brief 10 ms pulses uncontaminated by the slow tail current. By subtracting the appropriate Ca^{2+} current from each second-pulse current, the portion of the current attributable solely to the slow tail current was extracted. A plot of the resulting current–voltage curve is shown in Fig. 2*C*. The reversal potential of the tail current was −50 ± 5 mV ($n = 3$) with normal 4 mM extracellular K^+, and in one experiment was shifted to −23 mV in 10 mM K^+. The high-K^+ saline also increased the size of the tail, and virtually eliminated the sag current indicating that the initial voltage step was near the reversal potential. Assuming that K^+ and Cs^+ are the main ions contributing to the tail current, the reversal potentials can be used to calculate a relative permeability (P_{Cs}/P_K), which, in four experiments, was 0·22 ± 0·04.

The pharmacology of the tail current was investigated by extracellular application of some common K^+ channel

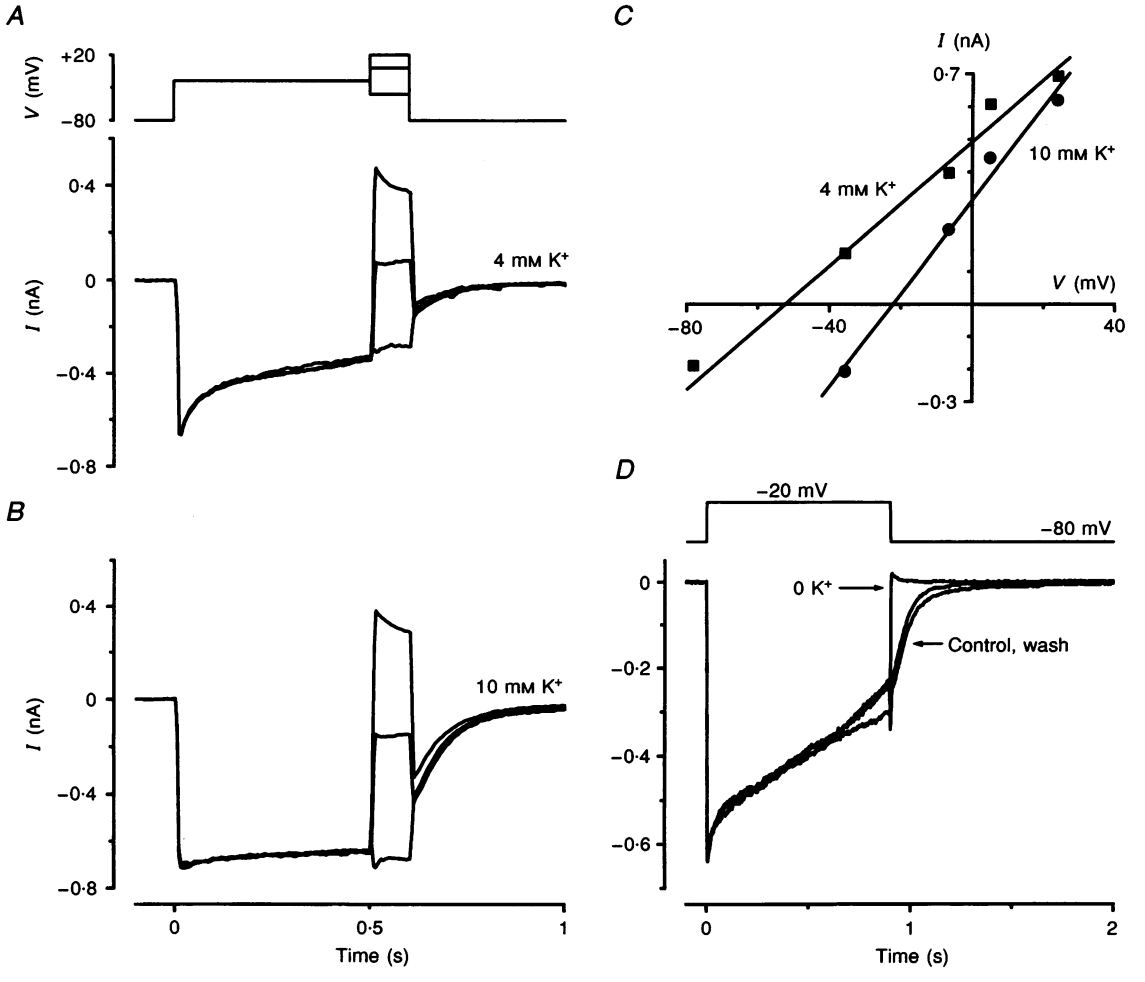

Figure 2. Ionic selectivity of tail current

A, double pulse experiment in 4 mM K^+; conditioning depolarization from −80 to −20 mV, followed by test steps to −40, 0 and +20 mV. *B*, double pulse experiment in 10 mM K^+; conditioning depolarization from −80 to −20 mV, followed by test steps to −40, 0 and +20 mV. *C*, current–voltage relationships from data in *A* and *B*; membrane potentials corrected for electrode series resistance and ohmic leak subtracted from currents. Fitted lines give reversal potentials of −23 mV (10 mM K^+) and −53 mV (4 mM K^+). *D*, currents recorded with Cs^+-based intracellular solution in response to depolarizing voltage steps from −80 to −20 mV; external solutions contain normal 4 mM K^+ (Control and wash) and zero K^+.

inhibitors. In four experiments the tail was blocked by local application of 0·1 μM apamin with a corresponding reduction in the sag current (Fig. 3*A*). Both tail and sag currents were also blocked by perfusion of TEA with a half-blocking concentration, K_i, of 5 mM (Fig. 3*C*). A small tail current that persisted in apamin and 50 mM TEA was removed in K^+-free saline suggesting that it results from incomplete channel block rather than from a separate current. The ionic selectivity and pharmacology of the tail current are inconsistent with the behaviour of previously characterized K^+ channels in turtle hair cells, especially the large conductance Ca^{2+}-activated K^+ (BK) channel which is impermeable to Cs^+, more sensitive to block by TEA ($K_i = 0{\cdot}3$ mM) and susceptible to charybdotoxin but not apamin (Latorre, Oberhauser, Labarca & Alvarez, 1989; Art *et al.* 1995). The data provide strong evidence for classifying the channel as an SK Ca^{2+}-activated K^+ channel.

Ca^{2+} dependence of tail current

The tail current grew progressively larger and longer with increasing pulse duration (Fig. 1) implying that it stemmed from Ca^{2+} accumulation within the cell. Several types of experiment were used to explore the role of Ca^{2+} in activating the tail current. Nifedipine, a blocker of L-type calcium channels, abolished both the Ca^{2+} current and the tail current (Fig. 4*A*) leaving only a small residual inward current during the pulse. Replacement of external Ca^{2+} with Ba^{2+}, which prevents BK channel activation (Art & Fettiplace, 1987), augmented the inward current but abolished the sag and tail currents suggesting that Ba^{2+}does not substitute for Ca^{2+} at the SK channel (data not shown). During extracellular perfusion of 1 μM Ca^{2+} saline, the Ca^{2+} current was replaced by a large inward current, carried by monovalent cations and having a rectangular shape without sag or tail (Art, Fettiplace & Wu, 1993). Finally, neither sag nor tail current was apparent when solutions in the recording pipette contained large concentrations of the Ca^{2+} buffer BAPTA (Fig. 9*D*). The results of the four types of experiment all argue that the K^+ tail current requires Ca^{2+} for its activation and is not purely voltage gated.

More quantitative information about the Ca^{2+} dependence of the tail current is shown in Fig. 4*B*. Depolarizations which activated the largest Ca^{2+} currents evoked the largest tail currents, and the sag in the inward current became steepest at peak calcium currents and potentials further from the reversal potential (−50 mV). To construct the current–voltage curve in Fig. 4*C*, the Ca^{2+} current was measured as the peak inward current at the start of the pulse, and the tail current was taken as the peak amplitude of the slow component at the end of the pulse. It should be noted that there was also a fast component of the tail current, due to inward Ca^{2+} current, but this rapid fraction decayed in less than 0·5 ms and was thus easily distinguishable from the much slower K^+ component. The slow tail's current–voltage curve has a similar U-shape to that of the Ca^{2+} current, indicating that the tail current activates along with the Ca^{2+} channels at around −50 mV, peaks at the same potential as the Ca^{2+} current, and is reduced with driving force on Ca^{2+} at positive potentials (Fig. 4*C*). The symmetry of the tail's current–voltage curve suggests that the Ca^{2+} affinity of the channel has little voltage sensitivity since different

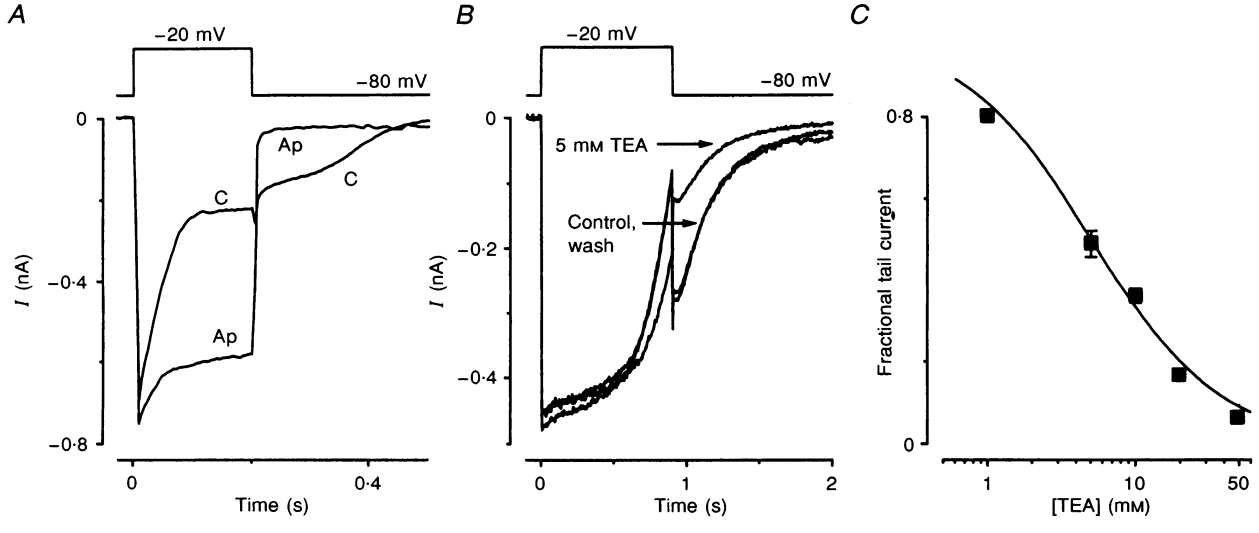

Figure 3. Apamin and TEA sensitivity of slow tail current

A, superimposed current traces recorded in control solution (C) and after a brief (10 s) application of 0·1 μM apamin (Ap) that blocks most of the sag during the pulse and the tail current. *B*, superimposed current traces before, during, and after external perfusion of saline containing 5 mM TEA, which halved the tail current and also reduced the sag. *C*, dose–response curve for TEA-block of tail current (data from 12 cells). The peak amplitude of the tail current immediately following the pulse during TEA perfusion was scaled to the peak amplitude in normal extracellular solution. The points were fitted by the Hill equation (continuous line) with $K_i = 5$ mM and Hill coefficient of 1.

depolarizations that evoke equivalent Ca^{2+} currents generate equivalent tails. There are several uncertainties which might distort the current–voltage curves in Fig. 4*C*, including underestimating the Ca^{2+} current by taking the initial peak inward current (see Fig. 3*A*) and underestimating the largest tail currents due to their saturation. Nevertheless, the results provide further support for the notion that the K^+ tail current requires Ca^{2+} for its activation.

Relationship between tail current and Ca^{2+} fluorescence

While the results in Fig. 4 demonstrate that the SK channel is reporting the intracellular Ca^{2+} concentration, they give no clue as to whereabouts in the cell the Ca^{2+} is being assayed. To address the question, the SK current was compared with the intracellular Ca^{2+} transients monitored with the fluorescent dye Calcium Green-5N, and viewed with a confocal microscope to improve spatial localization. As previously reported, the largest Ca^{2+} signals evoked by depolarization were found to be localized to submembranous regions in the basal half of the hair cell (Tucker & Fettiplace, 1995). In many cells these regions corresponded to a few small spots, each initially less than 1 μm in diameter. The spots grew brighter and larger throughout a depolarizing step and after repolarization they dissipated with two time constants of about 100 ms and 10 s. In other cells, a more or less continuous band of Ca^{2+} fluorescence was visible on each side of the cell in the basal half and it was less easy to distinguish discrete spots (Fig. 5). Outside these domains of high Ca^{2+}, especially towards the apical surface of the cell, the Ca^{2+} signals were relatively slow and small.

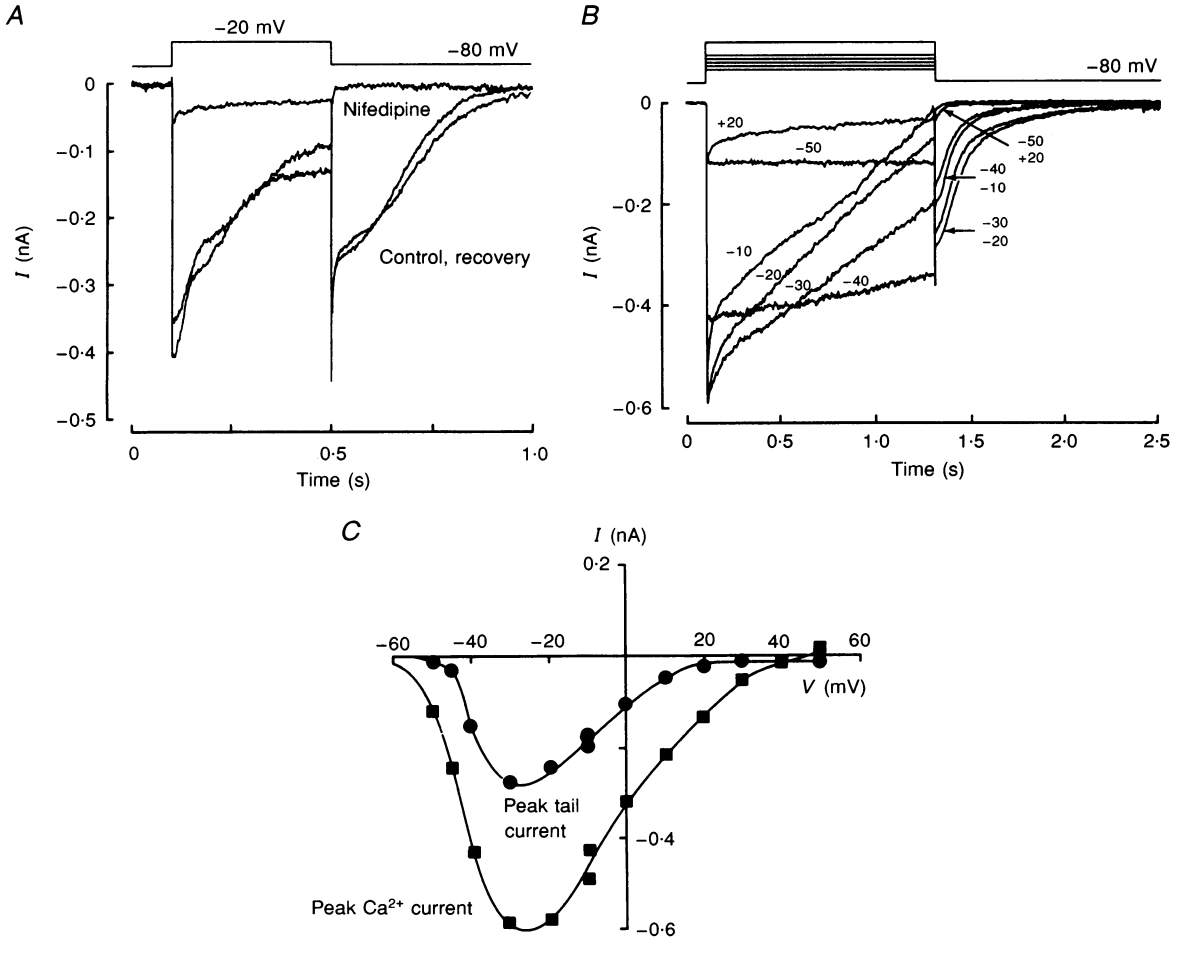

Figure 4. Calcium dependence of tail current

A, current traces before, during, and after application of 20 μM nifedipine, which blocks both the Ca^{2+} current and the slow tail current. *B*, superimposed current responses to voltage steps from −80 mV to the membrane potentials indicated by the traces. Note the correlation between the sizes of the Ca^{2+} current and the tail current. *C*, current–voltage relationships constructed from records in *B*, after ohmic leak had been subtracted. Ca^{2+} currents (■) were taken from the peak of the inward current immediately after the onset of the depolarization and tail currents (●) were measured by extrapolation of the slow tail component back to the end of the pulse.

A quantitative comparison of the time course of the Ca^{2+} fluorescence and the SK current is shown for two cells in Fig. 6. The fluorescence trace was obtained by monitoring a 2 μm diameter window overlaying the brightest region as shown in Fig. 5. The time course of the Ca^{2+} change at the SK channel was estimated as follows. First, the SK current was extracted from the whole-cell current by subtracting the Ca^{2+} current, which was assumed to be rectangular with amplitude equal to the peak inward current. Next, the tail current was inverted, and the sag current scaled to match the amplitude of the tail. This last manipulation was required to correct for the difference in driving force during and after the pulse. If a P_{Cs}/P_K of 0·22 was assumed without scaling, this gave something close to the same result. Finally, to obtain the Ca^{2+} concentration from the current, an assumption was needed about the Hill coefficient for Ca^{2+} binding to the SK channel. In about half the cells, there was a linear relationship between the SK current and the Ca^{2+} fluorescence; in the remainder of the cells an adequate match with the Ca^{2+} fluorescence could be achieved only by taking the square root of the current, indicating a Hill coefficient of at least 2. Examples of each category are shown in Fig. 6.

After these transformations, the time courses of the change in Ca^{2+} concentration derived from the SK current and from the fluorescence dye were comparable in the majority of cells over the first few hundred milliseconds. The major difference between the two time courses was that the SK tail current matched the fast component of the fluorescence decay, but not the slow component, and thus the quality of the agreement depended on the relative size of the slow component. While the tail current fully recovered in a few hundred milliseconds, a component of the fluorescence

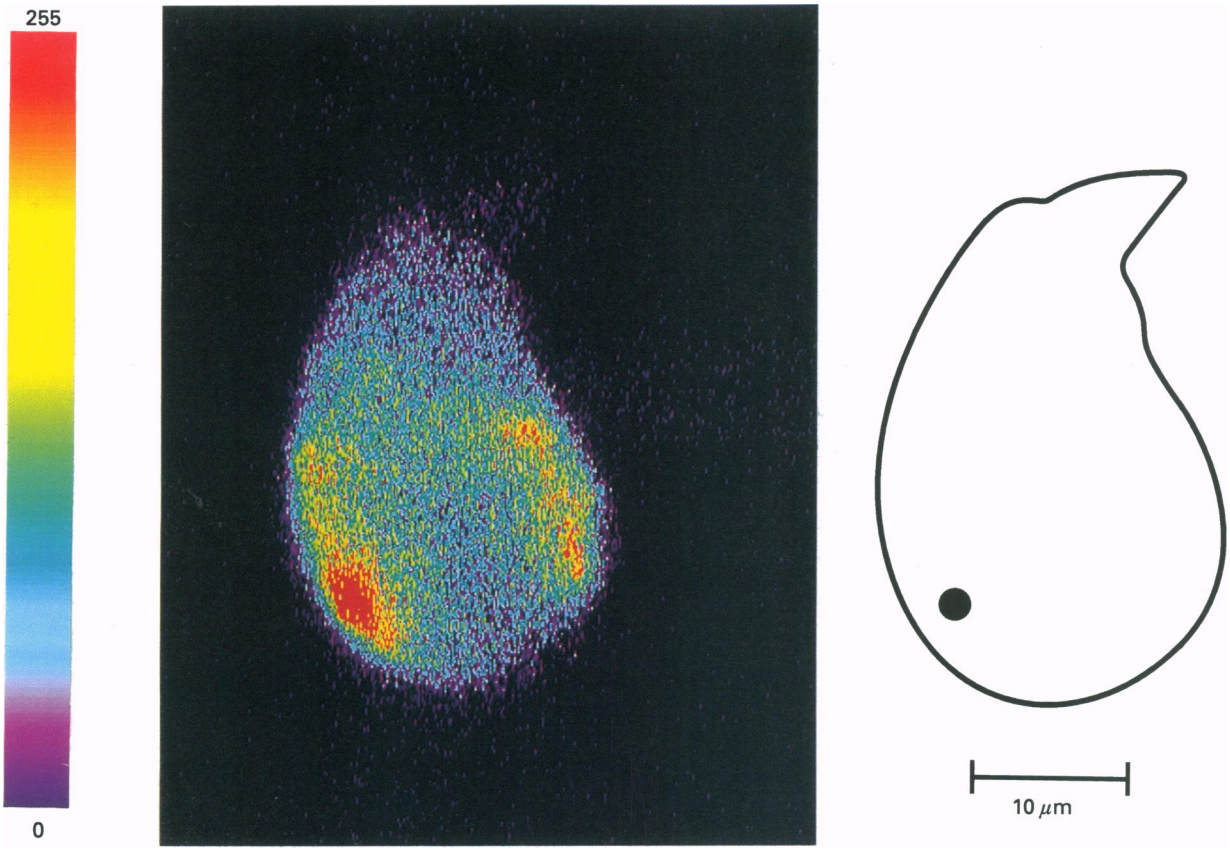

Figure 5. Calcium hotspots

Left, confocal image of a hair cell stained with 100 μM K_6-Calcium Green-5N. The image consists of the difference between the average images before and 300 ms after the onset of a voltage step from −80 to −20 mV. Note the higher fluorescence in regions along the sides of the basolateral membrane thought to be sites of Ca^{2+} entry. The hair bundle is at the top and the patch pipette, only faintly stained, is to the right. Right, schematic of the same hair cell, the circle denoting the 2 μm region where the time course of the fluorescence change was measured. The pseudocolour scale representing pixel intensity from 0 to 255 grey levels is shown on the left.

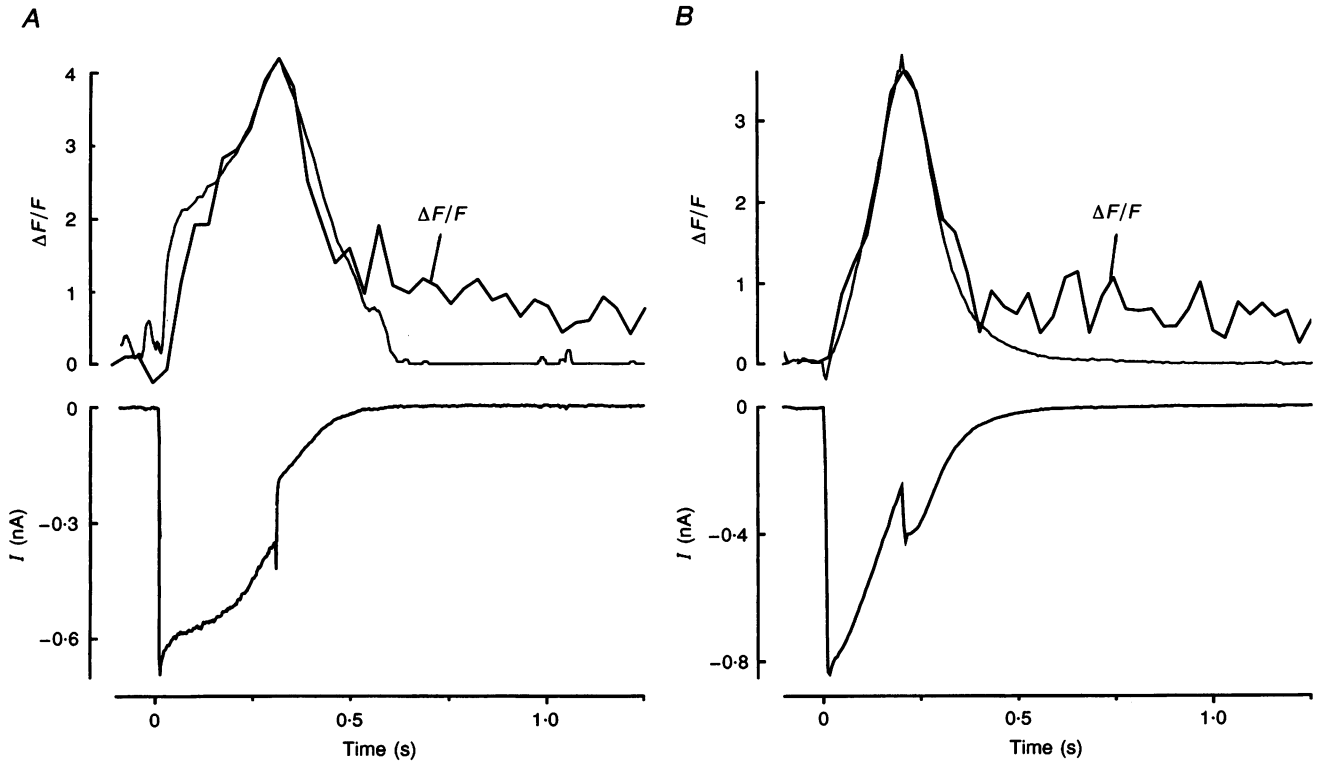

Figure 6. Comparison of the time course of the Ca^{2+} transient at a hotspot with the time course of the SK current

A, change in fluorescence for the cell of Fig. 5 in response to a 0·3 s depolarization from −80 to −20 mV, starting at time zero. The current record is shown below and the change in fluorescence, ΔF (normalized to the resting fluorescence F) is shown above for a 2 μm diameter region overlying the hotspot which is indicated in Fig. 5. Superimposed on the fluorescence trace is the time course of the intracellular Ca^{2+} transient deduced from the square root of the current record as described in the text. *B*, similar measurements on another cell for a 0·2 s depolarization from −80 to −20 mV. In this example the fluorescence trace was best matched by the SK current without taking the square root.

continued for tens of seconds. A measure of the similarity of the tail current and the hotspot Ca^{2+} was derived by comparing the decay time constants of the two processes in a number of cells. The time constant of Ca^{2+} recovery at the hotspot was obtained by fitting the fast component of the decline in fluorescence. The SK tail current was more difficult to quantify since it was not well fitted with a single exponential decay. Therefore the time for the tail current's amplitude to fall to 1/e was used as a measure of its duration. The collected measurements are plotted in Fig. 7. Multiple values are included for some cells before and after treatment with Ca^{2+}-ATPase inhibitors such as intracellular

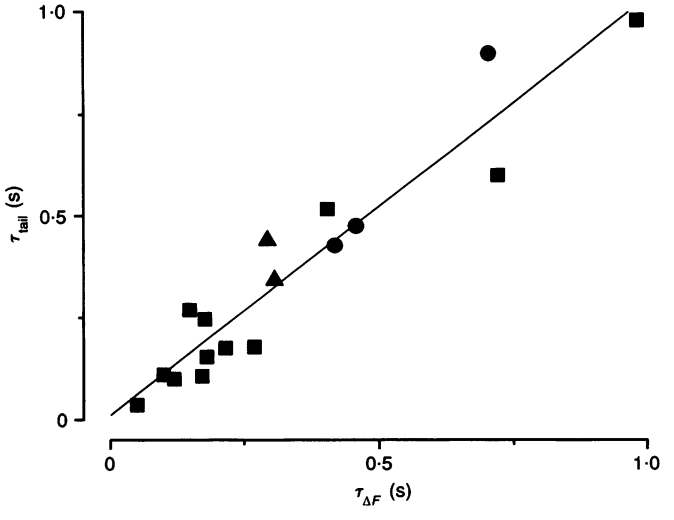

Figure 7. Plot of the decay time constant of the tail current against the decay time constant of the fast component of Ca^{2+} fluorescence

The abscissa value was obtained by fitting the initial component of the fluorescence decay. Owing to the complex time course of the tail current, the time constant on the ordinate was determined as the time from the end of the pulse for the tail current to decline to 1/e. Multiple measurements were made on some of the cells before (■) and after treatment with 1 mM intracellular vanadate (▲) or BHQ (●). These treatments prolonged both the Ca^{2+} transients and the SK tail currents. The fitted line had a slope of 1·0 and a regression coefficient of 0·952. Results of 12 cells illustrated.

vanadate and BHQ. As described in the next section these agents prevent Ca^{2+} clearance and hence lengthen the tail current. There is a good correlation in Fig. 7 between the Ca^{2+} decay derived in the two ways, the line through the points having a slope close to unity.

Role of calcium pumps

Imaging experiments in hair cells show that Ca^{2+} pump blockers increase the rate of expansion and slow the recovery of calcium fluorescence at hotspots, suggesting they impair Ca^{2+} removal (Tucker & Fettiplace, 1995). If the tail current monitors submembranous Ca^{2+}, it should be susceptible to the same perturbations. We have previously shown that intracellular perfusion with vanadate, an inhibitor of both intracellular and plasma membrane Ca^{2+}-ATPase pumps (Pedersen & Carafoli, 1987), increases the size and duration of the tail currents. Effects on the tails were visible at vanadate concentrations as low as 10 μM, and with 1 mM vanadate, the SK channels became permanently activated, indicating that the submembranous Ca^{2+} was no longer being cleared. The isoform of the Ca^{2+}-ATPase pump in intracellular membranes is selectively blocked by thapsigargin (Thastrup, Cullen, Drobak, Hanley & Dawson, 1990) and 2,5-di-(t-butyl)hydroquinone (BHQ; Kass, Duddy, Moore & Orrenius, 1989). During application of 0·3 μM thapsigargin, a progressive increase both in the sag during the pulse and in the size of the tails was observed in seven cells. In the example illustrated in Fig. 8*A*, the first measurement was taken 7 min after breakthrough, by which time the mobile buffers in the pipette (access resistance, 12 MΩ) and cell would have substantially equilibrated. The effect of thapsigargin then developed over the next 15 min. Perfusion of 10–100 μM BHQ also amplified and prolonged the tails (Fig. 8*B*), increasing the time required for the tail to recover from its peak amplitude to 1/e by a factor of 7·8 ± 5 ($n = 6$). Again, in the latter experiment, at least 5 min was allowed for the tail current to reach a steady state before presentation of the experiment was commenced. Furthermore, in the presence of either BHQ or thapsigargin, the tails eventually stabilized at new amplitudes, which were reproducible, arguing against cell degradation. However, the results confirm that manipulations influencing Ca^{2+} regulation, as shown with Ca^{2+} imaging experiments, produce parallel effects on the tail currents.

In a number of cells after treatment with Ca^{2+}-ATPase blockers, the tail current became flat-bottomed (e.g. Fig. 8*B*) remaining maximally activated for some time before returning to the baseline. This behaviour might arise if the Ca^{2+} concentration became sufficiently high to saturate all of the SK channels. Under these conditions, the maximum amplitude of the tail provides a measure of the total amount of SK conductance available. With all three Ca^{2+}-ATPase blocking agents, saturated tail currents of 0·4–0·8 nA were observed on repolarization to −80 mV. Assuming a reversal potential of −50 mV, these currents correspond to maximum conductances of between 13·5 and 27 nS.

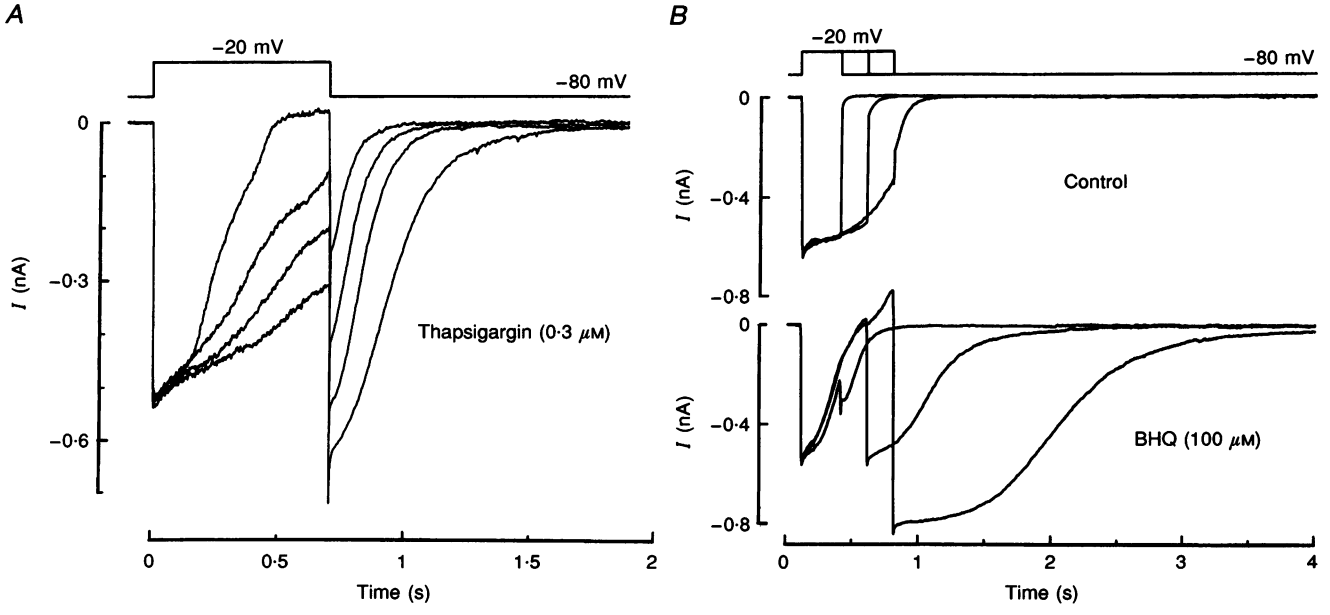

Figure 8. Effect of Ca^{2+}-ATPase inhibitors on the tail current

A, superimposed current traces recorded as 0·3 μM thapsigargin diffused from the pipette solution into the cell; records taken 7, 14, 18 and 22 min after breakthrough. With increasing time, the sag in inward current during the pulse became steeper and the amplitude of the tail current grew larger. *B*, current traces before (top) and after (bottom) extracellular perfusion with saline containing 100 μM 2,4-di-(t-butyl)hydroquinone (BHQ); depolarizing voltage steps from −80 to −20 mV for 300, 500 and 700 ms. The control records were taken after the responses had equilibrated, about 10 min after breakthrough. Note that with BHQ the tail current is much larger and longer lasting.

Estimation of the mobile endogenous calcium buffers

Mobile calcium buffers are an important factor in the cell's Ca^{2+} regulation, but measurement of their properties is complicated for a number of reasons. During whole-cell patch clamp, mobile buffers wash out of the cell leaving only fixed buffers. With the perforated-patch technique, which allows patch recordings without washout of large molecular mass cytoplasmic constituents, all buffers may be retained making it impossible to distinguish mobile and fixed fractions. The mobile buffer capacity may be assessed by comparing the Ca^{2+} signals recorded in a single cell under both perforated-patch and whole-cell conditions, in the presence and absence of mobile buffers. The Ca^{2+} signals can be quantified using fluorescent probes, but there are

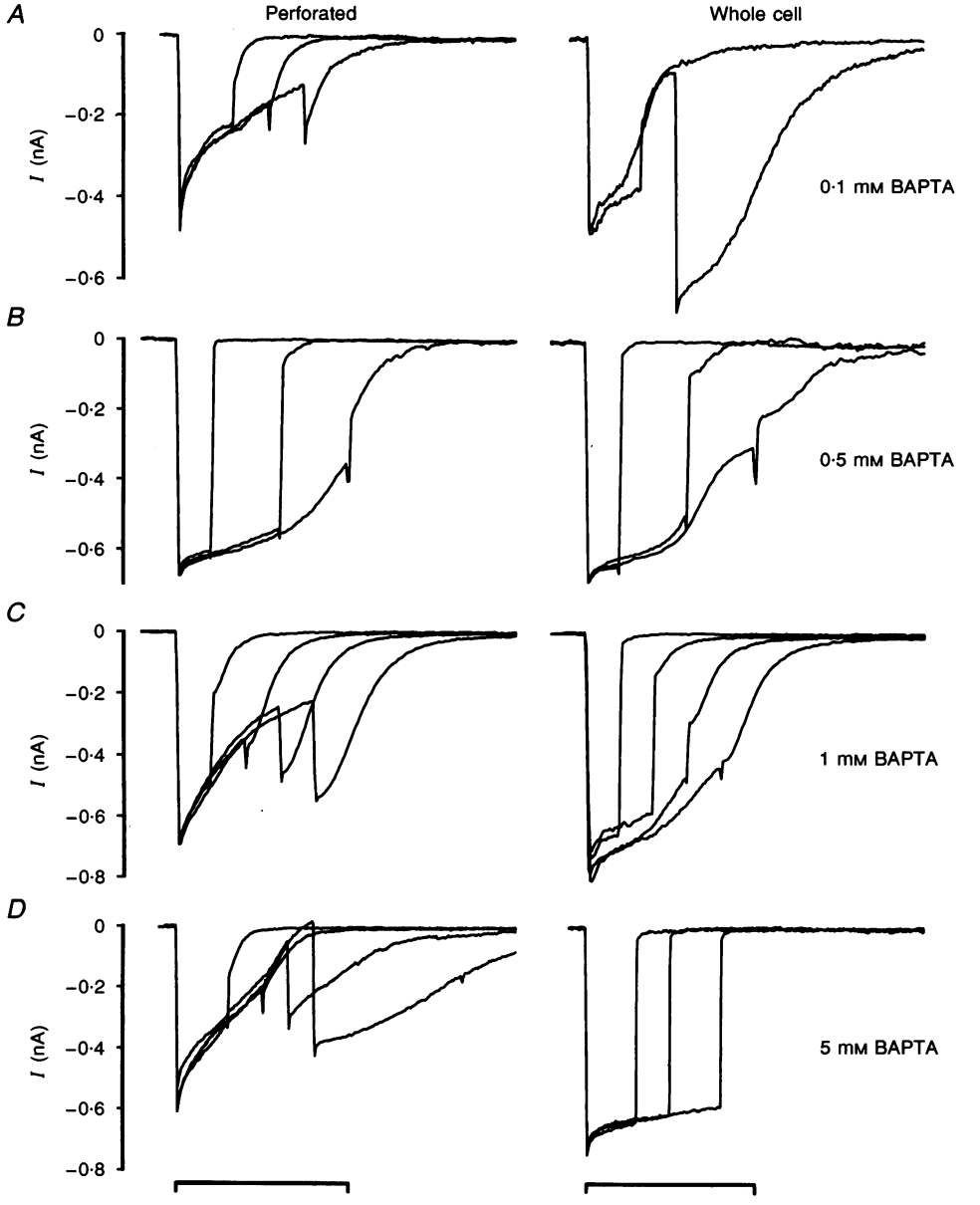

Figure 9. Comparison of mobile endogenous buffer with exogenous buffers before and after rupture of perforated-patch membrane

Left-hand column shows recordings from 4 cells made in the perforated-patch mode using amphotericin electrodes. The right-hand column gives the corresponding currents in the same cells about 10 min after breakthrough into whole-cell mode. The pipette solution contained different amounts of the Ca^{2+} buffer BAPTA, which are indicated beside the traces. For all current records the stimulus was a depolarization from −80 to −20 mV for several different durations. Calibration bar at the bottom marks 1 s (*B* and *C*) or 2 s (*A* and *D*).

complications with this procedure. Membrane-permeant dyes that stain a cell in the perforated-patch mode wash out in whole-cell mode, whereas dyes loaded through the pipette require patch rupture, and consequent washout of buffer. Whichever method is used to load the cell with dye, the transition from perforated-patch to whole-cell mode may alter the dye concentration and introduce error since the dye is a mobile buffer that adds to the binding capacity of the cell. The SK channel, an endogenous and immobile Ca^{2+} sensor, provides a means to bypass these complications.

Measurements were made initially in the perforated-patch configuration to observe tail currents in the presence of the mobile buffer. The patch was then ruptured to allow endogenous mobile buffer to wash out and exchange with the BAPTA in the pipette solution. During the subsequent 20 min of whole-cell recording, the tail current re-equilibrated enabling comparison of the pipette buffer with the cell's mobile buffer (Fig. 9). Experiments were conducted with BAPTA concentrations of between 0·1 and 5 mM in the pipette. As was found with nystatin (Zhou & Neher, 1993), the presence of intracellular polyene did not disrupt the cell's integrity for the duration of the recording, which lasted for at least 20 min following breakthrough.

In experiments using 0·1 mM BAPTA, the tail currents grew substantially after rupturing the patch, which indicates that an important buffering component was lost from the cell. Without this component, the SK channels report larger and longer calcium fluxes. In contrast, 5 mM BAPTA was sufficient to abolish the tails, suggesting that it is more powerful than the endogenous mobile buffer and able to capture Ca^{2+} faster than it can diffuse to the SK channels. The intermediate concentrations, 0·5 and 1 mM BAPTA, caused small changes in the tail that on average became larger in 0·5 mM and smaller in 1 mM. To make a quantitative comparison, each whole-cell tail current was integrated and normalized to the corresponding perforated-patch tail integral. The tail-integral ratios (whole cell/perforated) are plotted against the concentration of pipette buffer in Fig. 10 and the points have been fitted with a straight line. Interpolation of the abscissa value for a whole cell to perforated patch ratio of 1 indicates that the mobile endogenous buffer is equivalent to about 1 mM BAPTA.

When the pipette contained intermediate concentrations of BAPTA, the tail became smaller after rupture of the patch and required several minutes to grow to the final value. One explanation is that because of molecular mass differences, the pipette buffer is able to diffuse into the cell faster than a higher molecular mass endogenous buffer washes out. Although the slow pulse-repetition rate (1/90 s) made it difficult to measure accurately the time constant of exchange of the buffers, nevertheless some semi-quantitative observations can be made. At the highest BAPTA concentrations of 5 mM, the slow tail had disappeared by the time of the first or second test pulse, i.e. within 90–180 s after breakthrough. Using a molecular mass of 500 Da for BAPTA and a pipette access resistance of 20 MΩ, the 'wash-in' time constant, τ, is estimated as 95 s according to the empirical formula $\tau = 0{\cdot}6R_aM^{1/3}$, where τ is in seconds, R_a, the pipette access resistance, is in megaohms and M, the molecular mass of the diffusing species, is in daltons (Pusch & Neher, 1988). In four experiments where the pipette solution contained 0·1 or 0·5 mM BAPTA, the growth of the tail was largely complete on the fourth pulse, 6 min after breakthrough. Using a time constant of 6 min and a pipette resistance of 18 ± 6 MΩ, the calculated molecular mass for the endogenous buffer is 23·5 ± 6 kDa. This molecular mass is comparable to the 28 kDa of the purported endogenous buffer calbindin (Oberholtzer, Buettger, Summers & Matschinsky, 1988).

DISCUSSION

Characteristics and role of the SK channel

A variety of potassium channels have been characterized in turtle hair cells including the large-conductance calcium-activated potassium (BK) channel, the inwardly rectifying potassium (K_{IR}) channel, and the voltage-dependent delayed-

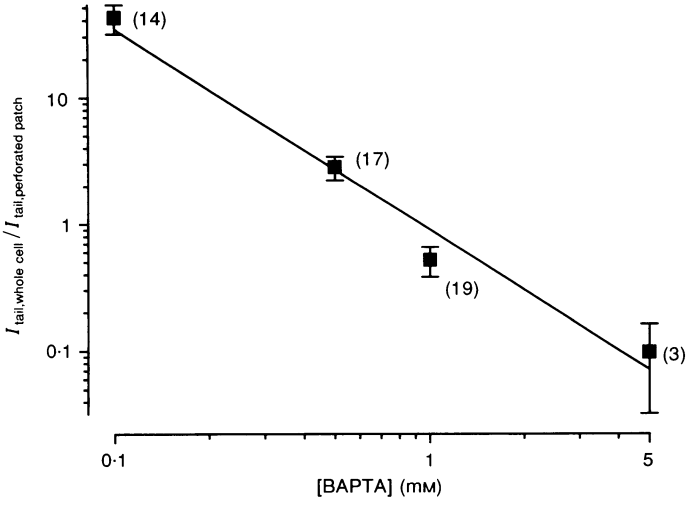

Figure 10. Estimation of the equivalent concentration of mobile endogenous Ca^{2+} buffer

For a given pulse duration, the tail current was integrated from records like those in Fig. 9 by calculating the area enclosed to the zero-current level for up to 5 s from the end of the pulse. The ordinate plots the ratio of the integral in whole-cell and in perforated-patch conditions with different concentrations of BAPTA as Ca^{2+} buffer in the intracellular solutions. Numbers of values averaged are given beside each point.

rectifier potassium (K_V) channel (Wu, Art, Goodman & Fettiplace, 1995; Goodman & Art, 1996). Here we have characterized a fourth potassium channel that is permeable to Cs^+ and K^+, blocked by apamin and TEA, and dependent on intracellular Ca^{2+}. These properties define it as an SK calcium-activated potassium channel (Blatz & Magleby, 1986; Latorre *et al.* 1989). This SK channel is likely to be the same channel previously observed in excised-patch recordings (Art *et al.* 1995), which had a single channel conductance of 30 pS in symmetrical K^+ and a voltage-independent Ca^{2+} affinity of about 2 μM. These characteristics of the SK channel distinguish it from the BK channel, which has a much larger single-channel conductance and a Ca^{2+} affinity of about 12 μM (at −50 mV) which depends on membrane potential (Art *et al.* 1995). Discovery of the SK channel in turtle hair cells helps explain the previous observation that to measure the Ca^{2+} current with Cs^+-filled electrodes, it was necessary to stimulate at a low repetition rate of 1 Hz (Art & Fettiplace, 1987); if faster rates were used, a 'leak conductance', presumably the SK conductance, quickly developed and obscured the Ca^{2+} current.

The SK channel may be the Ca^{2+}-activated K^+ channel found at the efferent synapse that is also permeable to Cs^+ but not NMG, and which is blocked by apamin, TEA and barium (Fuchs & Murrow, 1992; Erostegui, Nenov, Norris & Bobbin, 1994; Yuhas & Fuchs, 1995). Efferent stimulation evokes a slow hyperpolarizing IPSP in turtle hair cells which attenuates the receptor potential, and can eliminate the firing of afferent action potentials (Art, Fettiplace & Fuchs, 1984). The efferent terminals are thought to release acetylcholine, which increases intracellular Ca^{2+} and activates a K^+ current, but the proposed mechanisms disagree on the source of Ca^{2+}. The acetylcholine receptor may be nicotinic-like and coupled to an ion channel which is permeable to Ca^{2+} (Housley & Ashmore, 1991; Fuchs & Murrow, 1992), or muscarinic-like and use a second messenger such as IP_3 to release Ca^{2+} from an intracellular store (Shigemoto & Ohmori, 1990; Kakehata, Nakagawa, Takasaka & Akaike, 1993). Our observation that the SK channels can be activated by Ca^{2+} entering through voltage-gated channels reveals another Ca^{2+} source which can participate in inhibition. The results suggest that hair cells may have an internal mechanism for adaptation that is independent of the efferent projection, in which SK channels generate a graded hyperpolarization in response to large Ca^{2+} fluxes such as occur during intense auditory stimulation. Consistent with this idea, turtle hair cells can show, in response to loud, high-frequency tone stimuli, a slow adaptation of the receptor potential during the tone burst and a prolonged hyperpolarization at the end of the tone (see Fig. 10 of Crawford & Fettiplace, 1980). It is worth noting that the time courses of the after-hyperpolarization and of the efferent IPSP are both similar to the time course of the SK tail current, consistent with them all having a common origin.

Distribution of Ca^{2+} and SK channels

The overall similarity between the time course of the tail current and the fast decay of Ca^{2+} fluorescence (Fig. 6) suggests that the SK channels have a similar distribution to the hotspots which are confined to the basal half of the hair cell. Up to six hotspots were visible in confocal images of turtle hair cells (Tucker & Fettiplace, 1995) and we have previously suggested that the hotspots represent clusters of voltage-dependent Ca^{2+} channels, possibly localized to the synaptic release sites. Such clusters have been previously postulated on the basis of loose-patch recordings from bullfrog saccular hair cells (Roberts, Jacobs & Hudspeth, 1990). Since turtle hair cells in the mid-frequency region of the papilla possess, on average, about seventeen such release sites (Sneary, 1988), each hotspot would, in this explanation, correspond to the juxtaposition of multiple release sites; the inability to visualize individual release sites may stem from the slow time scales employed in confocal imaging during which diffusion of Ca^{2+} reduces spatial resolution. A different explanation would be that the hotspots are the sites of efferent synapses, of which there are between four and eight on the basolateral surface of turtle hair cells (Sneary, 1988). While the number of hotspots is comparable to the number of efferent synapses, there is neither evidence nor rationale for voltage-dependent Ca^{2+} channels being restricted to the efferent postsynaptic membrane. It seems more likely that the two channel types are spatially separate, with the Ca^{2+} channels being localized to the afferent release sites and the SK channels distributed in the membrane in the vicinity of the efferent terminals. One piece of evidence in favour of such a separation is the difference between the Ca^{2+} concentration required to half-activate the SK channel in detached patches (~2 μM; Art *et al.* 1995) and the Ca^{2+} concentration attained at the centre of the hotspots (up to 100 μM; Tucker & Fettiplace, 1995). This disparity suggests that the SK channel sees an attenuated version of the Ca^{2+} excursion at the centre of the hotspot. An alternative argument might be made that Ca^{2+} entering through channels near the afferent release sites diffuses to and releases Ca^{2+} regeneratively from the efferent subsynaptic cisternae, which thus appear as bright spots of high Ca^{2+} concentration. This explanation also seems unlikely in view of the linear relationship between the Ca^{2+} current and the Ca^{2+} concentration at the hotspot (see Fig. 3 of Tucker & Fettiplace, 1995).

Variability in the tail current

There was significant variability between cells in the amplitude and time course of the tail current and their relationship to pulse duration. The tail amplitude in mid-frequency hair cells varied between 0·1 and 0·8 nA for a standard 300 ms pulse, but if the pulse was extended, or the Ca^{2+} buffering reduced so that the tail appeared saturated, a more restricted current spread of 0·4–0·8 nA was observed (see Figs 8 and 9*A*). This range presumably reflects a variation in the number of SK channels per cell.

However, it is worth noting that the presence of a sigmoidal onset to the tail symptomatic of its saturation was not a reliable indicator of the point at which the current was maximal; often some saturation was evident well below the maximum current level (see Fig. 8*B*). One explanation for this kinetic behaviour is that the SK channels are at a variable distance from the Ca^{2+} source and, consequently, nearby SK channels saturate before those channels that are more distant from the source. Such variation would make the tail current difficult to define kinetically, and could also impair the match with the fluorescence results. It would also explain the differences between the traces in experiments like those in Fig. 1. There the tail current shows some saturation at 0·4 nA for the longest pulse in Fig. 1*A*, but not under the same conditions for another cell in Fig. 1*B*. A third type of variability was in the dependence of the tail amplitude on pulse duration: two different cells might possess the same number of SK channels, but one would require a longer pulse to achieve the maximal tail amplitude than the other. Differences in the concentration of Ca^{2+} buffer contained in different hair cells could contribute to this type of variability (see below).

Calcium buffers

As a voltage-independent, non-inactivating Ca^{2+} detector, the SK channel is a useful tool for monitoring submembranous Ca^{2+}. It provided us with a method to measure the endogenous mobile buffer bypassing the complications associated with calcium dyes; and by combining perforated-patch and whole-cell measurements on single cells, we were able to avoid making comparisons between different cells. A convincing demonstration that a mobile buffer shapes submembrane signals is shown by the small tails in perforated-patch mode and the larger tails in whole-cell mode with 0·1 mM BAPTA (Fig. 9). The interpretation is that an endogenous buffer binds calcium before it reaches SK channels in perforated-patch mode, but washes out during whole-cell access allowing larger calcium fluxes at the channel. By varying the concentration of exogenous buffer in the pipette, we determined that 1 mM BAPTA has a binding capacity equivalent to the endogenous mobile buffer, virtually identical to the values reported in frog saccular hair cells (Roberts, 1993). The Ca^{2+}-binding capacity, β, of a buffer, B, can be calculated from $\beta = d[Ca^{2+}\text{–}B]/d[Ca^{2+}]$ (Neher & Augustine, 1993). In the Ca^{2+} concentration range below the K_D, $\beta \approx [B]/K_D$, where [B] is the concentration of buffer and K_D its affinity for Ca^{2+}. The identity of the endogenous buffer may be 28 kDa calbindin-D which is one of the most abundant proteins in hair cells (Oberholtzer *et al.* 1988) and is thought to have four Ca^{2+}-binding sites with an affinity of about 1 μM (Bredderman & Wasserman, 1974). The binding capacity for 1 mM BAPTA ($K_D = 0{\cdot}2$ μM) is 5000, and to match this buffering power, the calbindin concentration must also be close to 1 mM. However, this concentration may represent only an average value and hair cells tuned to higher frequencies might be expected to have more diffusible Ca^{2+} buffer to match their larger complement of Ca^{2+} channels (Art *et al.* 1993).

In the absence of mobile buffer, the cytoplasm maintains a significant ability to buffer Ca^{2+}. In previous calcium-imaging experiments (Tucker & Fettiplace, 1995), the fixed buffer was estimated to have a binding capacity over 200, with low affinity binding that remained linear up to 10 μM free Ca^{2+}. This buffer has yet to be identified and may include multiple components, but it does not include cytoplasmic organelles containing Ca^{2+}-ATPases, which were inhibited in these experiments. If the fixed buffer were a single component with K_D of 10 μM, it would have a concentration of approximately 2 mM. Intracellular organelles, including mitochondria (Baker & Umbach, 1987) and endoplasmic reticulum, by sequestering Ca^{2+} also contribute to the buffering capacity of the cytoplasm. Organelles have the advantage that they can be localized to specific regions of the cell and can thus behave as a non-uniformly distributed sink supplementing the fixed buffer. Most of these organelles contain Ca^{2+}-ATPase pumps (Schatzmann, 1989) that are blocked by thapsigargin and BHQ. The actions of these inhibitors which: (i) cause the Ca^{2+} hotspots to expand faster and further (Tucker & Fettiplace, 1995); and (ii) exaggerate the SK tail currents, suggest that intracellular compartments play a significant role in hair cell Ca^{2+} homeostasis.

Art, J. J. & Fettiplace, R. (1987). Variation of membrane properties in hair cells isolated from the turtle cochlea. *Journal of Physiology* **385**, 207–242.

Art, J. J., Fettiplace, R. & Fuchs, P. A. (1984). Synaptic hyperpolarization and inhibition of turtle cochlear hair cells. *Journal of Physiology* **360**, 397–421.

Art, J. J., Fettiplace, R. & Wu, Y.-C. (1993). The effects of low calcium on the voltage-dependent conductances involved in tuning of turtle hair cells. *Journal of Physiology* **470**, 109–126.

Art, J. J., Wu, Y.-C. & Fettiplace, R. (1995). The calcium-activated potassium channels of turtle hair cells. *Journal of General Physiology* **105**, 49–72.

Baker, P. F. & Umbach, J. A. (1987). Calcium buffering in axons and axoplasm of *Loligo*. *Journal of Physiology* **383**, 369–394.

Barish, M. E. & Thompson, S. H. (1983). Calcium buffering and slow recovery kinetics of calcium-dependent outward current in molluscan neurons. *Journal of Physiology* **337**, 201–219.

Blatz, A. L. & Magleby, K. L. (1986). Single apamin-blocked Ca-activated K^+ channels of small conductance in rat skeletal muscle. *Nature* **323**, 718–720.

Bredderman, P. J. & Wasserman, R. H. (1974). Chemical composition, affinity for calcium, and some related properties of the Vitamin D dependent calcium-binding protein. *Biochemistry* **13**, 1687–1694.

Crawford, A. C. & Fettiplace, R. (1980). The frequency selectivity of auditory nerve fibres and hair cells in the cochlea of the turtle. *Journal of Physiology* **306**, 79–125.

Erostegui, C., Nenov, A. P., Norris, C. H. & Bobbin, R. P. (1994). Acetylcholine activates a K^+ conductance permeable to Cs^+ in guinea pig outer hair cells. *Hearing Research* **81**, 119–129.

Fuchs, P. A. & Murrow, B. W. (1992). Cholinergic inhibition of short (outer) hair cells of the chick's cochlea. *Journal of Neuroscience* **12**, 800–809.

Goodman, M. B. & Art, J. J. (1996). Positive feedback by a potassium-selective inward rectifier enhances tuning in vertebrate hair cells. *Biophysical Journal* (in the Press).

Hodgkin, A. L., McNaughton, P. A. & Nunn, B. J. (1987). Measurement of sodium–calcium exchange in salamander rods. *Journal of Physiology* **391**, 347–370.

Housley, G. D. & Ashmore, J. F. (1991). Direct measurement of the action of acetylcholine on isolated outer hair cells of the guinea pig cochlea. *Proceedings of the Royal Society of London* B **244**, 161–167.

Kakehata, S., Nakagawa, T., Takasaka, T. & Akaike, N. (1993). Cellular mechanism of acetylcholine-induced response in dissociated outer hair cells of guinea-pig cochlea. *Journal of Physiology* **463**, 227–244.

Kass, G. E., Duddy, S. K., Moore, G. A. & Orrenius, S. (1989). 2,5-Di-(tert-butyl)-1-4-benzohydroquinone rapidly elevates cytosolic Ca^{2+} concentration by mobilizing the inositol 1,4,5-trisphosphate-sensitive Ca^{2+} pool. *Journal of Biological Chemistry* **264**, 15192–15198.

Latorre, R., Oberhauser, A., Labarca, P. & Alvarez, O. (1989). Varieties of calcium-activated potassium channels. *Annual Review of Physiology* **51**, 385–399.

Llinás, R., Sugimori, M. & Silver, R. B. (1992). Microdomains of high calcium concentration in a presynaptic terminal. *Science* **256**, 677–679.

Neher, E. & Augustine, G. J. (1992). Calcium gradients and buffers in bovine chromaffin cells. *Journal of Physiology* **450**, 273–301.

Oberholtzer, J. C., Buettiger, C., Summers, M. C. & Matschinsky, F. M. (1988). The 28-kDa calbindin-D is a major calcium binding protein in the basilar papilla of the chick. *Biochemistry* **85**, 3387–3390.

Pawley, J. B. (1995). Fundamental limits in confocal microscopy. In *Handbook of Confocal Microscopy*, 2nd edn, ed. Pawley, J. B., pp. 19–37. Plenum Press, London.

Pedersen, P. L. & Carafoli, E. (1987). Ion motive ATPases. I. Ubiquity, properties and significance for cell function. *Trends in Biochemical Sciences* **12**, 146–150.

Pusch, M. & Neher, E. (1988). Rates of diffusional exchange between small cells and a measuring patch pipette. *Pflügers Archiv* **411**, 204–211.

Rae, J., Cooper, K., Gates, P. & Watsky, M. (1991). Low access resistance perforated patch recordings using amphotericin B. *Journal of Neuroscience Methods* **37**, 15–26.

Roberts, W. M. (1993). Spatial calcium buffering in saccular hair cells. *Nature* **363**, 74–76.

Roberts, W. M., Jacobs, R. A. & Hudspeth, A. J. (1990). Colocalization of ion channels involved in frequency selectivity and synaptic transmission in presynaptic active zones of hair cells. *Journal of Neuroscience* **10**, 3664–3684.

Schatzmann, H. (1989). The calcium pump of the surface membrane and the SR. *Annual Review of Physiology* **51**, 473–485.

Shigemoto, T. & Ohmori, H. (1991). Muscarinic receptor hyperpolarizes cochlear hair cells of chick by activating Ca^{2+}-activated K^+ channels. *Journal of Physiology* **442**, 669–690.

Smith, S. & Augustine, G. (1988). Calcium ions, active zones and synaptic transmitter release. *Trends in Neurosciences* **11**, 458–464.

Sneary, M. G. (1988). Auditory receptor of the red-eared turtle. II. Afferent and efferent synapses and innervation patterns. *Journal of Comparative Neurology* **276**, 588–606.

Thastrup, O., Cullen, P. J., Drobak, B. K., Hanley, M. R. & Dawson, A. P. (1990). Thapsigargin, a tumor promoter, discharges intracellular Ca^{2+} stores by specific inhibition of the endoplasmic reticulum Ca^{2+} ATPase. *Proceedings of the National Academy of Sciences of the USA* **87**, 2466–2470.

Tucker, T. & Fettiplace, R. (1995). Confocal imaging of calcium microdomains and calcium extrusion in turtle hair cells. *Neuron* **15**, 1323–1336.

Wu, Y.-C., Art, J. J., Goodman, M. B. & Fettiplace, R. (1995). A kinetic description of the calcium-activated potassium channel and its application to electrical tuning of hair cells. *Progress in Biophysics and Molecular Biology* **63**, 131–158.

Yau, K.-Y. & Nakatani, K. (1984). Electrogenic Na-Ca exchange in retinal rod outer segments. *Nature* **311**, 661–663.

Yuhas, W. A. & Fuchs, P. A. (1995). Acetylcholine activates apamin-sensitive K^+ channels in chick cochlear hair cells. *Society for Neuroscience Abstracts* **21**, 1824.

Zhou, Z. & Neher, E. (1993). Mobile and immobile calcium buffers in bovine adrenal chromaffin cells. *Journal of Physiology* **469**, 245–273.

Acknowledgements

This work was supported by a research grant (5 R01 DC01362) to R.F. from the National Institutes on Deafness and Other Communication Disorders, National Institutes of Health. We should like to thank Jon Art, Tony Ricci, Larry Trussell and Mike Wu for commenting on the manuscript.

Author's email address

R. Fettiplace: fettiplace@neurophys.wisc.edu

Received 5 January 1996; accepted 11 April 1996.